Shap. Mem. Superelasticity (2022) 8:277–294
https://doi.org/10.1007/s40830-022-00382-1

TECHNICAL ARTICLE

A Shape Memory Alloy Constitutive Model with Polynomial Phase Transformation Kinetics

Arthur Adeodato[1] · Lucas L. Vignoli[2] · Alberto Paiva[3] · Luciana L. S. Monteiro[1] · Pedro M. C. L. Pacheco[1] · Marcelo A. Savi[4]

Received: 23 April 2022 / Revised: 5 July 2022 / Accepted: 24 July 2022 / Published online: 17 August 2022
© ASM International 2022

Abstract Shape memory alloys (SMAs) have a complex thermomechanical behavior due to the variety of strong nonlinear phenomena involved. In this regard, the SMA constitutive modeling is still a challenging topic even after several relevant research efforts related to that. Among these possibilities, there is a class of constitutive model that assumes the phase transformation kinetics, combining simplicity with good results. This work proposes a novel constitutive model with polynomial phase transformation kinetics where the main advantage is to explicitly evaluate either stress-driven or strain-driven cases avoiding iterative algorithms. This approach is of special interest for several situations, including dynamical applications and finite element analysis. Numerical simulations are carried out showing the model capabilities to describe the thermomechanical behavior of SMAs. Initially, the model is compared with quasi-static experimental tests showing a good agreement. Afterward, dynamical analysis is developed considering a single-degree of freedom oscillator indicating the model ability to capture the main features of the SMA nonlinear dynamics .

Keywords Shape memory alloys · Constitutive model · Nonlinear dynamics · Experimental characterization · Numerical simulations

This invited article is part of a special issue of *Shape Memory and Superelasticity* honoring Etienne Patoor for his contributions to the field of phase-transforming materials and shape memory alloys. The special issue was organized by Dr. Fodil Meraghni, Ecole Nationale Supérieure d'Arts et Métiers (Arts et Métiers Institute of Technology), and Dr. Dimitris Lagoudas, Texas A&M University.

✉ Marcelo A. Savi
savi@mecanica.coppe.ufrj.br

[1] Department of Mechanical Engineering, Centro Federal de Educação Tecnológica Celso Suckow da Fonseca, CEFET/RJ, Rio de Janeiro 20.271.110, Brazil

[2] Center for Technology and Application of Composite Materials, Department of Mechanical Engineering, Universidade Federal do Rio de Janeiro, Macaé, Rio de Janeiro, Brazil

[3] Department of Mechanical Engineering, Escola de Engenharia de Volta Redonda, Universidade Federal Fluminense, Volta Redonda, RJ 27.255.250, Brazil

[4] Center for Nonlinear Mechanics, COPPE - Department of Mechanical Engineering, Universidade Federal do Rio de Janeiro, P.O. Box 68.503, Rio de Janeiro 21.941.972, Brazil

Introduction

Shape memory alloy (SMA) remarkable properties have been motivating several applications in different areas of human knowledge. Aerospace and robotics are some areas with distinct examples using SMAs as actuators or passive elements, including structural morphing [1]. Biocompatibility of NiTi alloys make them attractive for medical and dentistry areas [2–4]. Drug delivery [5, 6], stents [7], and wound closure [8] are some other biomedical applications of SMAs.

SMA properties are essentially related to adaptive temperature-dependent behavior associated with microstructural phase transformations that generates effects as shape memory and pseudoelasticity. SMA actuators can impose either forces or displacements when subjected to thermomechanical loads. Jani et al. [9] presented a review about recent progresses and developments associated with shape memory alloy actuators. Monteiro et al. [10, 11] evaluated different SMA actuator configurations and the effect of thermomechanical couplings. Oliveira et al. [12]

discussed some aspects of the thermomechanical characterization of SMA actuators.

Bioinspiration is a design strategy that extracts concepts from biological and natural systems. The use of smart materials in general, and in particular shape memory alloys, is an essential point for this design possibilities. Vaidyanathan et al. [13] employed shape memory alloy elements to actuate bioinspired devices. Lee et al. [14] used origami-inspired structures to develop an adaptive device that is able to change its form and shape according to environmental conditions. Copaci et al. [15] developed a new flexible SMA actuator that provides movement to wearable robots. The design of exoskeleton prototypes demonstrated the utility and advantages offered in mechanical actuators to improve the comfort and adaptability. Brandão and Savi [16] discussed the use of SMAs in tensegrity systems to build a human foot prosthesis.

Dynamical systems are another interesting possibility to exploit the adaptive behavior of SMAs. In essence, temperature-dependent behavior is exploited by considering either property changes or hysteretic dissipation. Besides, SMA dynamical systems present rich and complex behaviors [17]. SMA oscillators are employed to describe this complex behavior and, since the pioneer work of Savi and Braga [18], several studies evaluated the details of the SMA oscillator behaviors described by different constitutive models. Savi and Pacheco [19] exploited chaos and hyperchaos in oscillators with one- and two-degree of freedom systems considering a polynomial constitutive model. Savi et al. [20] employed a more sophisticated constitutive model showing hysteretic behavior and tension–compression asymmetry. Bernardini and Vestroni [21] investigated thermomechanical couplings and dynamical jumps. Bernardini and Rega [22, 23] explored the occurrence of chaos in shape memory oscillators, emphasizing some of the main dynamical characteristics of these systems. The influence of thermomechanical coupling on the rate-dependent mechanical response are discussed establishing a systematic numerical investigation based on an enhanced version of the Method of Wandering Trajectories [24]. Bernardini and Rega [25] investigated the influence of the constitutive model on nonlinear dynamics of SMA oscillators. Results show that, for single-degree of freedom oscillators, different models can give similar dynamical response, although with the exception of different transient behaviors. However, different models can present distinct trends through frequency response analysis.

Aguiar et al. [26] presented an experimental investigation showing SMA adaptive dynamical behavior, confirming numerical predictions of the response of SMA oscillators. Enemark et al. [27] experimentally evaluated the influence of different external stimuli, load frequencies, and ambient temperatures in dynamical systems with SMA helical spring elements. As part of the experimental analysis, spring behavior is an essential point to characterize the dynamical system. In this regard, it is important to highlight some articles dealing with SMA helical springs. Aguiar et al. [28] discussed the main principles of SMA helical spring modeling, confirming results with experimental data. Enemark et al. [29] and Savi et al. [30] discussed the influence of geometrical nonlinearities on SMA helical springs. Viet et al. [31] investigated the influence of spring index for SMA springs.

Rotordynamic systems are another application where SMAs have been applied. Borges et al. [32] investigated the dissipation associated with pseudoelastic springs for active control of a rotor-bearing system. Alves et al. [33] exploited the influence of shape memory alloys on the dynamic behavior of flexible rotors. A suspension composed by shape memory alloy wires connected to a rotor-bearing test rig was designed to evaluate system performance. Results show that phase transformation can promote the suspension stiffness variation confirming that SMA is an interesting alternative for vibration control.

The general concept of vibration attenuation using SMAs is of special interest for many other dynamical applications [17, 34–37]. Li and Feng [38] analyzed the influence of temperature and mechanical loads in a frequency response showing the shift of the resonance peak. Doaré et al. [39] explored high levels of strain observing dynamical jumps in a pseudoelastic torsional system. Souza and de Marqui [40] combined vibration attenuation with energy harvesting in typical airfoil with superelastic springs combined with piezoelectric elements, attenuating vibrations related to aerodynamic flutter. Adeodato et al. [41] also investigated the synergistic use of SMA–piezoelectric material for energy-harvesting purposes. Silva et al. [42] exploited the SMA capability to dissipate energy and decrease stick–slip issues in drilling operations. Structures subjected to seismic excitations is another topic where SMAs are showing to be interesting. Saadat et al. [43] and Han et al. [44] presented overviews of seismic applications of SMAs. Wang et al. [45] and Varela and Saiddi [46] performed an experimental analysis of vibration attenuation devices. Vignoli et al. [47] investigated the use of hybrid composites with pseudoelastic elements for vibration attenuation in earthquake structures.

All these applications need a proper mathematical description in order to develop an appropriate design that can exploit all system details. In this regard, constitutive modeling is an essential point for the use of SMAs, being a challenging problem due to several complex phenomena involved. Several research efforts have been performed for the mathematical description of the thermomechanical behavior of SMAs. Paiva and Savi [48], Lagoudas [36],

Cisse et al. [49], and Patoor et al. [50, 51] presented general overviews of the main initiatives related to SMA constitutive models. The new challenging topics of the SMA description include 3D modeling [52–56], plasticity [57–60], anisotropy [61], load rate influence [62–64], tension–compression asymmetry [30, 57, 65], functional [66–68], and structural [69] fatigue.

Concerning SMA composites, Zhu et al. [70] modeled self-healing application in metal matrix composites. Viet and Zaki [71] evaluated functionally graded SMA bars. Viet et al. [72] discussed the influence of the SMA positions in a composite beam and Viet et al. [73] extended this investigation for beams combining SMA and piezoelectric materials.

Based on the literature review of SMA constitutive models, an important class of model is the assumed phase transformation kinetics, which the main characteristic is the use of known functions to describe the phase transformation kinetics. Tanaka et al. [74] presented the pioneer work of this kind of model, using exponential expressions for phase transformation kinetics. Afterward, alternatives were developed considering different possibilities of the phase transformation function [27, 48, 49, 74–78]. Brinson [75] proposed a new version of the assumed phase transformation kinetics incorporating some essential improvements to the model.

This work proposes a novel constitutive model for SMAs considering a polynomial phase transformation kinetics, following the well-established assumed phase transformation kinetics framework. The main advantage of the proposed model is the possibility to avoid iterative procedures for strain-driven and stress-driven cases. This approach is of special interest for either dynamical applications or finite element analysis. The paper presents the novel model and, afterward, the experimental characterization, discussing the identification of the constitutive parameters. Quasi-static tests are simulated showing the model capabilities to describe the general thermomechanical behavior of SMAs. A dynamical system analysis is developed considering a single-degree of freedom oscillator indicating the model ability to capture the main features of the SMA nonlinear dynamics.

Constitutive Model

SMA constitutive models with assumed phase transformation kinetics is a class of model that has a broad use, adopting a mathematical expression to describe the phase transformation kinetics. The constitutive equation considers the state variables, stress, σ, strain, ε, temperature, T, and the internal variable, $\xi = \xi_S + \xi_T$ that represents martensitic volume fraction, where ξ_S is the stress-induced detwinned martensite and ξ_T is the temperature-induced twinned martensite. It is assumed that the sign of ξ defines the martensitic variant. Therefore, $-1 \leq \xi_S \leq +1$ and $0 \leq \xi_S \leq +1$ represent the tensile detwinned martensitic variant M^+, while $-1 \leq \xi_S \leq 0$ represents the compressive detwinned martensitic variant M^-. The following constitutive equation is proposed in the rate form and for one-dimensional media:

$$\dot{\sigma} = E\dot{\varepsilon} + c\dot{\xi}_S + \Theta\dot{T}; \tag{1}$$

where E is the Young's modulus, $\Theta = Ea$ is a thermal coefficient with a representing the thermal expansion coefficient, and $c = -E\varepsilon_R$ with ε_R representing the maximum recoverable strain coefficient.

The rate form equation can be integrated, being expressed as follows:

$$\sigma = \sigma_0 + (E\varepsilon - E_0\varepsilon_0) + (c\xi_S - c_0\xi_{S0}) + (\Theta T - \Theta_0 T_0); \tag{2}$$

where the index "0" indicates the initial state.

Phase transformation kinetics is described by considering a mathematical expression for forward, austenite–martensite transformation $A \rightarrow M$ and reverse, martensite–austenite transformation $M \rightarrow A$. Each one of them is defined by critical stress levels that are functions of temperature. Basically, critical stress defines a hypersurface in stress–temperature space, similar to the plastic yield surface, defining the phase transformation region. In general, it is important to identify the start and finish of austenite–martensite phase transformation, σ_{Ms} and σ_{Mf}; and the start and finish of martensite-austenite phase transformation, σ_{As} and σ_{Af}. Experimental observations reveal a linear temperature dependence for high temperatures, which is the original assumption of most of the models [76]. Nevertheless, low-temperature behavior shows a different pattern where critical stress can be considered constant [75]. Figure 1 presents the critical phase transformation stress surfaces and their temperature dependence for these two situations. M_s and M_f are the start and finish temperatures for martensitic transformation in a stress-free state, while A_s and A_f are the start and finish temperatures for the reverse transformations in a stress-free state.

The general description for the phase transformation critical stresses are defined as follows:

$$\begin{aligned} \sigma_{Ms} &= \sigma_1 + C_M(T - M_s) \\ \sigma_{Mf} &= \sigma_2 + C_M(T - M_s) \\ \sigma_{As} &= C_A(T - A_s) \\ \sigma_{Af} &= C_A(T - A_f) \end{aligned}; \tag{3}$$

where σ_1 and σ_2 are constant values for start and finish critical stresses to represent austenite–martensite phase transformations observed in temperatures below M_s [75].

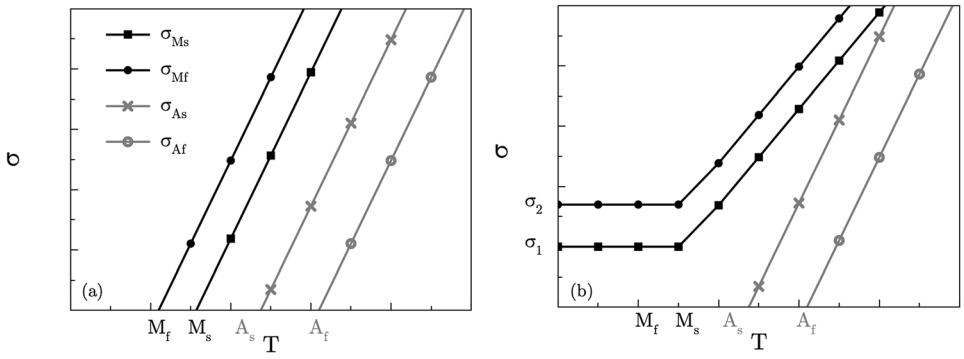

Fig. 1 Phase transformation stress surfaces as a function of temperature: **a** model by Liang and Rogers [76] and **b** model by Brinson [75]

Based on that the phase transformation kinetics is described in proper regions, being expressed by the following general equations:

$$\beta = \beta_0 + (1-\beta_0) f_M(\sigma,T) \quad \begin{cases} A \rightarrow M^-, M^+ \\ M \rightarrow M^+, M^- \end{cases} \tag{4}$$

$$\beta = \beta_0 f_A(\sigma,T) \qquad M, M^-, M^+ \rightarrow A; \tag{5}$$

where $0 \le \sigma \le 1$ and $0 \le T \le 1$ are normalized stress and temperature, defined as follows for each phase transformation.

$$\sigma = \frac{\sigma - \sigma_{Ms}}{\sigma_{Mf} - \sigma_{Ms}} \quad \begin{cases} A \rightarrow M^+, M^- \\ M \rightarrow M^+, M^- \end{cases}; \qquad T = \frac{T - M_s}{M_f - M_s} \quad A \rightarrow M \tag{6}$$

$$\sigma = \frac{\sigma - \sigma_{Af}}{\sigma_{As} - \sigma_{Af}} \quad M^+, M^- \rightarrow A \qquad T = \frac{T - A_f}{A_s - A_f} \quad M, M^+, M^- \rightarrow A \tag{7}$$

The hardening functions $f_M(\sigma,T)$ and $f_A(\sigma,T)$ define phase transformation kinetics, and different expressions are proposed in the literature. The original work of Tanaka et al. [74] proposed an exponential law. Liang and Rogers [76] proposed trigonometric functions adopting the same critical transformation stress values, expressed as a linear function. Brinson [75] improved the models with assumed transformation kinetics dividing the volume fraction into two distinct martensitic fractions, one induced by temperature and other induced by stress: $\beta = \beta_T + \beta_S$. Under this assumption, the model establishes a distinction between twinned martensite (M) and detwinned martensite ($M^?$ or M^-). Besides, a more realistic description is employed to describe the critical phase transformation stress values, as presented in Fig. 1b. Different Young's modulus for austenite and martensite are assumed and, therefore, a rule of mixtures is employed, being expressed by

$$E = E_A + \beta(E_M - E_A): \tag{8}$$

Enemark et al. [27, 29] proposed a change into hardening functions assuming Bézier polynomial functions, which is more effective to describe internal subloops presenting good agreement with experimental data.

The models with transformation kinetics have the characteristic that the hardening functions are expressed as a function of stress and temperature. Hence, stress-driven case is directly evaluated but strain-driven case needs to be associated with a proper iterative algorithm [17]. A novel model with polynomial kinetics is proposed in order to avoid iterative procedure for both stress-driven and strain-driven cases.

On this basis, consider that the hardening functions $f_M(\sigma,T)$ and $f_A(\sigma,T)$ are expressed by two successive second-order polynomial equations. The general form of the polynomial equation is defined with the aid of a variable κ that represents σ and T:

$$f_M(\kappa) = \begin{cases} a_1\kappa^2 + b_1\kappa + c_1 & 0 \le \kappa \le B_M \\ a_2\kappa^2 + b_2\kappa + c_2 & B_M < \kappa \le 1 \end{cases} \tag{9}$$

$$f_A(\kappa) = \begin{cases} a_3\kappa^2 + b_3\kappa + c_3 & 0 \le \kappa \le B_A \\ a_4\kappa^2 + b_4\kappa + c_4 & B_A < \kappa \le 1 \end{cases} \tag{10}$$

where $0 < B_M < 1$ and $0 < B_A < 1$ are controlling parameters for forward and reverse transformations, respectively, defining start and finishes of the polynomial curve. In this regard, the hardening functions are the following:

$$\beta_S = \begin{cases} \beta_{S0} + (1-\beta_{S0})(a_1\sigma^2) & \text{if } \sigma \le B_M \\ \beta_{S0} + (1-\beta_{S0})(a_2\sigma^2 + b_2\sigma + c_2) & \text{if } \sigma > B_M \end{cases} \quad \begin{cases} A \rightarrow M^+, M^- \\ M \rightarrow M^+, M^- \end{cases} \tag{11}$$

$$\beta_S = \begin{cases} \beta_{S0}(a_3\sigma^2 + b_3\sigma + c_3) & \text{if } \sigma \le B_A \\ \beta_{S0}(a_4\sigma^2) & \text{if } \sigma > B_A \end{cases} \quad M^+, M^- \rightarrow A; \tag{12}$$

$$\beta_S = \begin{cases} \beta_{S0}(a_3 T^2 + b_3 T + c_3) & \text{if } T \le B_A \\ \beta_{S0}(a_4 T^2) & \text{if } T > B_A \end{cases} \quad M^+/M^- \to A; \tag{13}$$

$$\beta_T = \begin{cases} \beta_{T0} + (1-\beta_{T0})(a_1 T^2) & \text{if } T \le B_M \\ \beta_{T0} + (1-\beta_{T0})(a_2 T^2 + b_2 T + c_2) & \text{if } T > B_M \end{cases} \quad A \to M; \tag{14}$$

$$\beta_T = \begin{cases} \beta_{T0}(a_3 T^2 + b_3 T + c_3) & \text{if } T \le B_A \\ \beta_{T0}(a_4 T^2) & \text{if } T > B_A \end{cases} \quad M \to A: \tag{15}$$

On this basis, polynomial coefficients need to be estimated, which is discussed in the sequel. By considering martensite–austenite phase transformation, one needs to have $f_M(0) = 0$ and $f_M(1) = 1$ and also considering that horizontal tangent at start and finish of the curve must be satisfied ($df_M(0)/d\xi = 0$ and $df_M(1)/d\xi = 0$). Continuity condition has to be considered in $f_M(B_M)$ and its derivatives with respect to ξ and $df_M/d\xi(B_M)$, at connection point. Under these assumptions, $b_1 = 0$ and $c_1 = 0$ and the other coefficients are defined by the following linear system:

$$\begin{bmatrix} 0 & 1 & 1 & 1 \\ 0 & 2 & 1 & 0 \\ B_M^2 & -B_M^2 & -B_M & -1 \\ 2B_M & -2B_M & -1 & 0 \end{bmatrix} \begin{Bmatrix} a_1 \\ a_2 \\ b_2 \\ c_2 \end{Bmatrix} = \begin{Bmatrix} 1 \\ 0 \\ 0 \\ 0 \end{Bmatrix}. \tag{16}$$

By solving the equations, one can find the coefficients:

$$\begin{aligned} a_1 &= \frac{1}{B_M} \\ a_2 &= \frac{1}{B_M - 1} \\ b_2 &= -\frac{2}{B_M - 1} \\ c_2 &= \frac{B_M}{B_M - 1} \end{aligned}. \tag{17}$$

Leading to the stress–strain relation for forward phase transformation as follows:

$$\begin{aligned} &(\beta_0 - 1)a_1 \left(\frac{\xi - \xi_{Ms}}{\xi_{Mf} - \xi_{Ms}}\right)^2 + \xi - a\beta_0 - \varepsilon_0 \\ &-E\varepsilon + E_0\varepsilon_0 + a_0\beta_0 = 0 \quad \text{if } 0 \le \frac{\xi - \xi_{Ms}}{\xi_{Mf} - \xi_{Ms}} \le B_M \end{aligned} \tag{18}$$

$$\begin{aligned} &(\beta_0 - 1)a_2 \left(\frac{\xi - \xi_{Ms}}{\xi_{Mf} - \xi_{Ms}}\right)^2 + (\beta_0 - 1)b_2 \left(\frac{\xi - \xi_{Ms}}{\xi_{Mf} - \xi_{Ms}}\right) + \xi - a\beta_0 \\ &+(\beta_0 - 1)c_2 a - \varepsilon_0 - E\varepsilon + E_0\varepsilon_0 + a_0\beta_0 = 0 \quad \text{if } B_M \le \frac{\xi - \xi_{Ms}}{\xi_{Mf} - \xi_{Ms}} \le 1 \end{aligned} \tag{19}$$

For reverse transformation, $f_A(1) = 1$ and $f_A(0) = 0$. Horizontal tangent at start and finish of the curve must be satisfied ($df_A(1)/d\xi = 0$ and $df_A/d\xi(0) = 0$), and continuity has to be considered at the connection point B_A ($f_A(B_A)$ and $df_A(B_A)/d\xi$). Since $b_4 = 0$ and $c_4 = 0$, the system is reduced to

$$\begin{bmatrix} 1 & 1 & 1 & 0 \\ 2 & 1 & 0 & 0 \\ B_A^2 & B_A^2 & 1 & -B_A^2 \\ 2B_A & 1 & 0 & -2B_A^2 \end{bmatrix} \begin{Bmatrix} a_2 \\ b_3 \\ c_4 \\ a_4 \end{Bmatrix} = \begin{Bmatrix} 1 \\ 0 \\ 0 \\ 0 \end{Bmatrix}. \tag{20}$$

By solving the equation, one finds the coefficients for the reverse transformation:

$$\begin{aligned} a_3 &= \frac{1}{B_A - 1} \\ b_3 &= -\frac{2}{B_A - 1} \\ c_3 &= -\frac{B_A}{B_A - 1} \\ a_4 &= \frac{1}{B_A} \end{aligned}. \tag{21}$$

Leading to the stress–strain relation for reverse phase transformation as follows:

$$\begin{aligned} &-\beta_0 a_3 \left(\frac{\xi - \xi_{Af}}{\xi_{As} - \xi_{Af}}\right)^2 - \beta_0 b_3 \left(\frac{\xi - \xi_{Af}}{\xi_{As} - \xi_{Af}}\right) + \xi - \beta_0 c_3 a \\ &-\varepsilon_0 - E\varepsilon + E_0\varepsilon_0 + a_0\beta_0 = 0 \quad \text{if } B_A \le \frac{\xi - \xi_{Af}}{\xi_{As} - \xi_{Af}} \le 1 \end{aligned} \tag{22}$$

$$\begin{aligned} &-\beta_0 a_4 a \left(\frac{\xi - \xi_{Af}}{\xi_{As} - \xi_{Af}}\right)^2 + \xi - \varepsilon_0 - E\varepsilon + E_0\varepsilon_0 + a_0\beta_0 \\ &= 0 \quad \text{if } 0 \le \frac{\xi - \xi_{Af}}{\xi_{As} - \xi_{Af}} \le B_A; \end{aligned} \tag{23}$$

where the SMA Young's modulus is updated for each step.

It should be pointed out that for strain-driven cases, the constitutive equation becomes a simple quadratic polynomial and the stress can be directly computed using Baskara equation. On the other hand, for stress-driven case, the martensitic volume fraction is directly computed. Variables and parameters with index "0" represent initial conditions. These values are updated after load direction inversion and when the load crosses the origin point.

The novel polynomial model has the advantage to present analytical solution for strain-driven simulations since a closed form equation can be established, avoiding an iterative algorithm to estimate stress values from the strain.

The other models with assumed phase transformation kinetics employ a predictor–correct scheme where a trial state is defined from strain values.

Experimental Characterization

The characterization of an SMA specimen is performed considering thermomechanical tests and an SMA Sandinox wire with u = 0:9 mm diameter and $L_0 = 220$ mm length is employed. Characterization starts with a Differential Scanning Calorimeter (DSC) test (Netzsch DSC 200 F3) with the aim to identify phase transformation temperatures. An SMA wire sample (5–15 l g) is tested considering a prescribed temperature and monitoring the necessary energy. Results are presented in Fig. 2 highlighting the critical phase transformation temperatures.

Mechanical characterization is carried out considering quasi-static mechanical load and unload at different temperatures. A wire with $L_0 = 220$ mm length is of concern using 60 mm to clamp the wire in each side. An INSTRON 5982 universal testing machine is employed considering controlled displacement rate of 4.5 mm/min for 5 cycles total. The SMA wire deformation is estimated using the crosshead displacement. A training process is employed before the tests imposing a series of 20 cycles. Stress–strain diagrams are presented in Fig. 3 showing typical pseudoelastic behavior associated with high temperature and martensite reorientation related to low-temperature behavior.

These experimental tests allow the estimation of all constitutive parameters. Young's modulus can be estimated by considering the slope of the linear portions before and after phase transformations, based on procedures presented in [30]. Different moduli are estimated for martensitic and austenitic phases. Austenitic phase modulus is measured at high temperature (T [A_f) via linear interpolation of points in range from 20 to 30% of maximum load for austenitic phase. Similarly, points from 80 to 90% of maximum load are considered for linear interpolation for the martensitic modulus. This methodology reduces the influence of instability effects related to experimental measurements at the beginning of the test and at the load reversal regions. For low temperatures ($T = 243$ K), points from 5 to 10% are considered for linear interpolation. Critical stress phase transformations are estimated by considering the same procedure. Linear interpolations are carried out in order to estimate the start and finish of phase transformation points. Figure 4 presents the auxiliary pictures for the estimation of phase transformation critical stress values and elastic modulus for different temperatures.

Based on the critical phase transformation stress values evaluated at different temperatures, it is possible to build the critical phase transformation stress surfaces, presented in Fig. 5.

Once the model considers constant phase transformation critical stresses for temperatures below M_s, red points in Fig. 5 indicate a theoretical value assumed for $T = 243$ K. It is also noticeable that red lines are built by the linear interpolation of experimental results. For this reason, they do not coincide with the theoretical points showed in Fig. 1.

Table 1 summarizes the constitutive parameters characterized by the thermomechanical tests. Austenitic and martensitic elastic modulus are determined by the arithmetic mean of measured values in Fig. 4. In addition, C_A and C_M are estimated by the mean of respective slopes presented in Fig. 5. In addition, thermal expansion is neglected in the presence of phase transformations and therefore, thermal coefficient is X = 0. The next section is

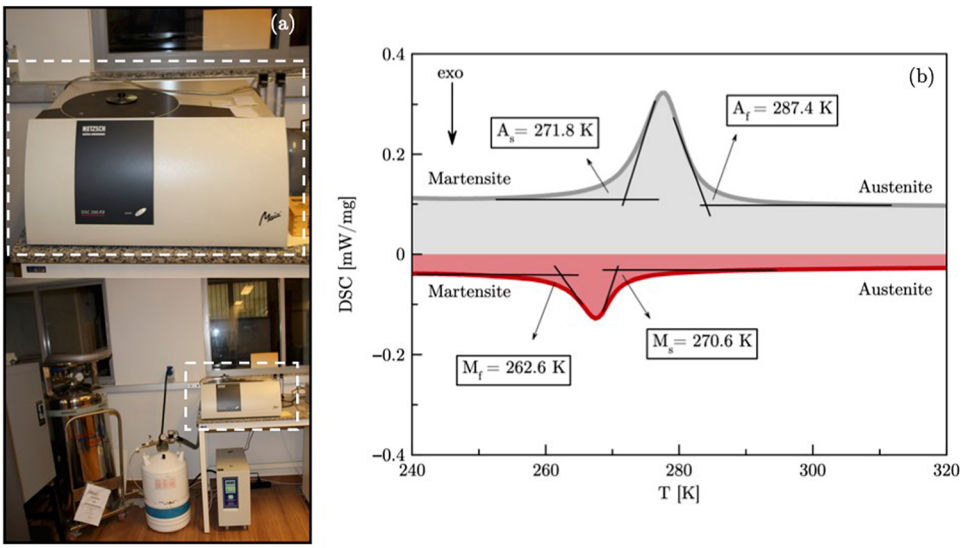

Fig. 2 Phase transformation temperature characterization: **a** DSC tests experimental setup and **b** differential scanning calorimetry of pseudoelastic wire sample u = 0:9 mm

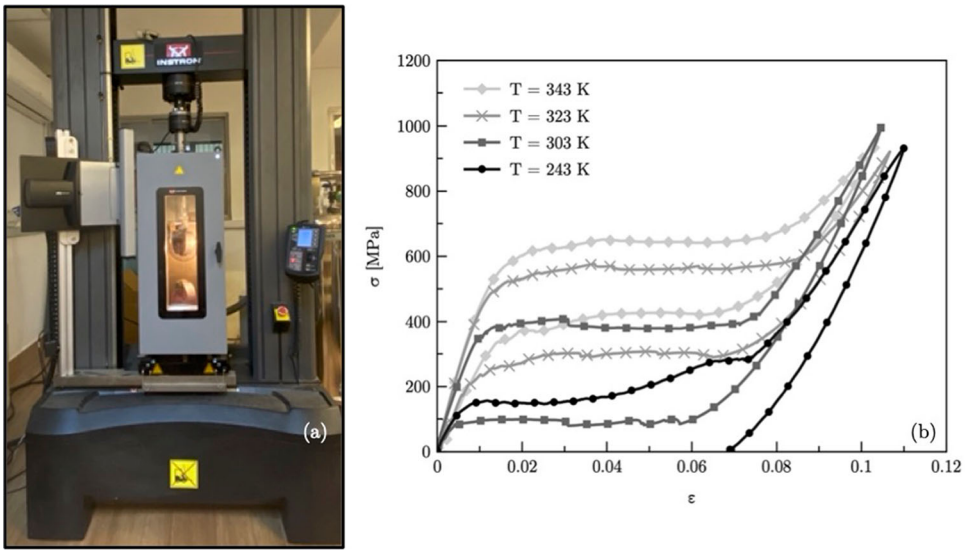

Fig. 3 Mechanical test characterization: **a** tensile tests experimental setup and **b** experimental stress–strain curves for different temperature conditions

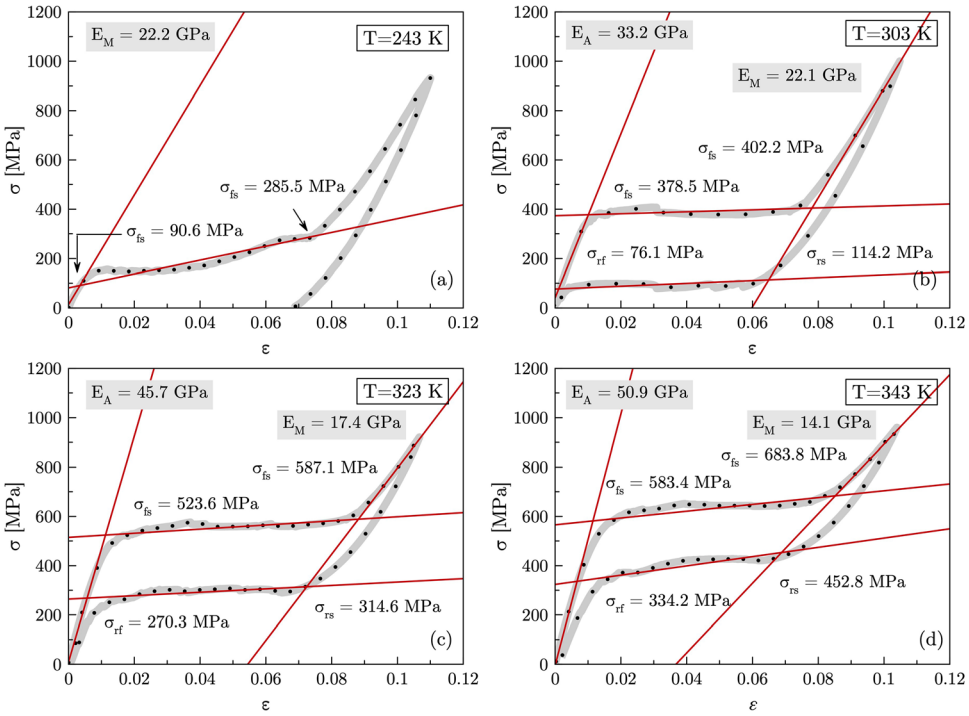

Fig. 4 Experimental determination of SMA Young's modulus and critical stress phase transformations: **a** $T = 243$ K; **b** $T = 303$ K; **c** $T = 323$ K; and **d** $T = 343$ K

dedicated to evaluate the novel model considering quasi-static tests that are compared with experimental data.

Quasi-static Tests

Numerical simulations of quasi-static tests are now of concern. The idea is to attest the model capability to describe the thermomechanical behavior of the SMAs comparing results of the numerical simulations with experimental data. Numerical results are obtained by considering strain-driven cases with incremental step De= 0.001 and a maximum strain of 0.1. Figure 6 shows the comparison between numerical simulations with experimental data presented in the previous section for different temperatures. Both martensite reorientation for low-temperature behavior and pseudoelastic effect for high-temperature behavior are captured by the model considering $B_M = 0{:}6$ and $B_A = 0{:}4$. Note that hysteresis loop shifts up with the increase of temperature.

Figure 7 presents the influence of some different adjustments of the model parameters B_M and B_A. Figure 7a presents the stress–strain curve at constant temperature $T = 303$ K, showing the pseudoelastic effect. On the other

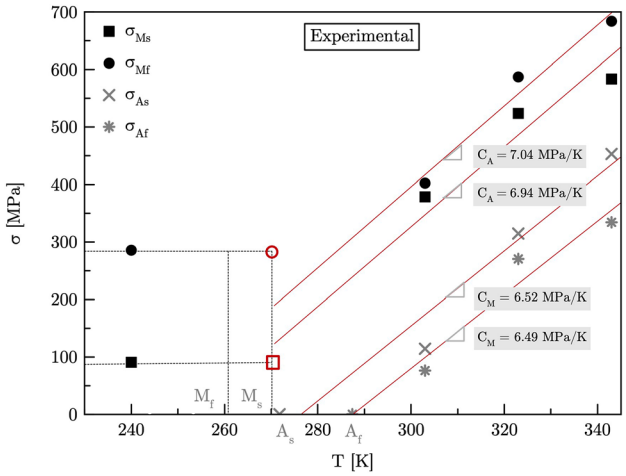

Fig. 5 Experimental critical phase transformation stress surfaces as a function of temperature

Table 1 Experimental parameters for SMA wire sample

M_s (K)	M_f (K)	A_s (K)	A_f (K)	r_s (MPa)	r_f (MPa)
270.6	262.6	271.8	287.4	90.6	285.5
E_A (GPa)	E_M (GPa)	C_A (MPa/K)	C_M (MPa/K)	ε_R	
43.2	18.9	7	6.5	0.06	

hand, Fig. 7b shows temperature-induced phase transformation at a constant vanishing stress.

The ability of the proposed model to describe internal subloops due to incomplete phase transformations is now of concern. Figure 8 presents results associated with high-temperature condition, $T = 303$ K, which characterizes a pseudoelastic effect. Figure 8a shows stress–strain curves considering both tensile and compression loads and internal subloops due to incomplete phase transformations. Figure 8b shows prescribed strain, Fig. 8c shows elastic modulus, and Fig. 8d presents the evolution of martensitic volume fraction. Note that the sign of b defines the martensitic variant and when b\ 0, compressive variant is of concern. Results presents coherent behavior in qualitative agreement with experimental tests.

Temperature-induced phase transformation is now of concern considering an SMA sample subjected to temperature variations with a null-stress state. Figure 9 presents results in the form of strain–temperature curves, the evolution of strain, and martensitic volume fraction, together with the prescribed temperature.

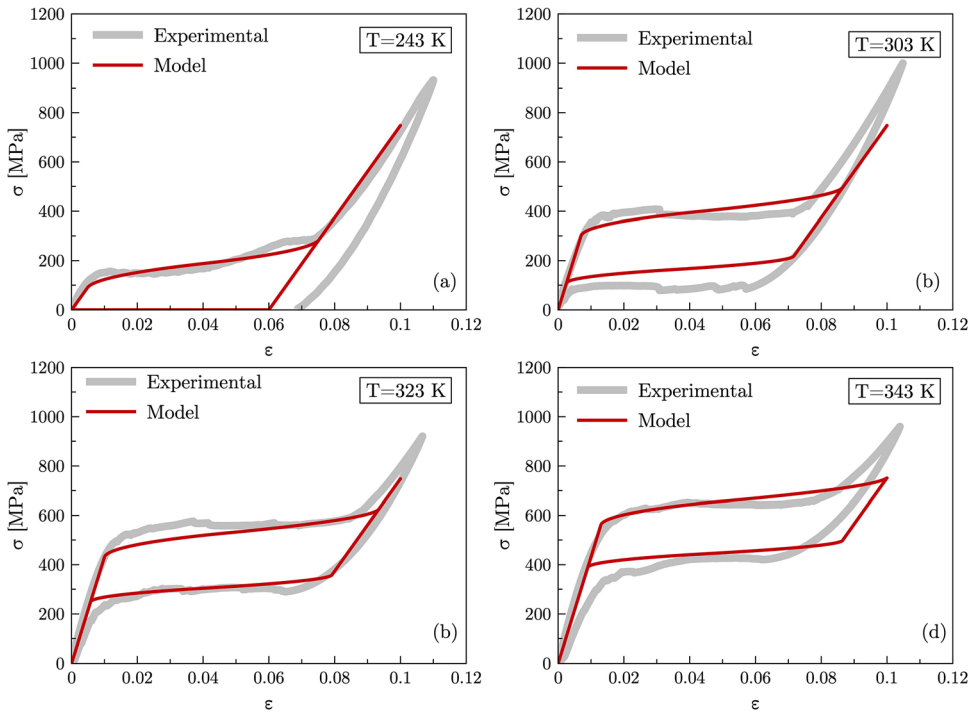

Fig. 6 Polynomial phase transformation model compared with experimental data for different temperature conditions: **a** $T = 243$ K; **b** $T = 303$ K; **c** $T = 323$ K; and **d** $T = 343$ K

Fig. 7 Analysis of constitutive parameters B_M and B_A: **a** mechanical-induced phase transformation and **b** temperature-induced phase transformation

Fig. 8 Pseudoelastic behavior with internal subloops for $T[\ A_f$: **a** stress–strain curve; **b** strain-driven history; **c** Young's modulus; and **d** martensite volume fraction

Fig. 9 Temperature-induced behavior considering internal subloops for $T\backslash\ M_s$: **a** strain–temperature curve; **b** temperature-driven history; **c** strain; and **d** martensitic volume fraction

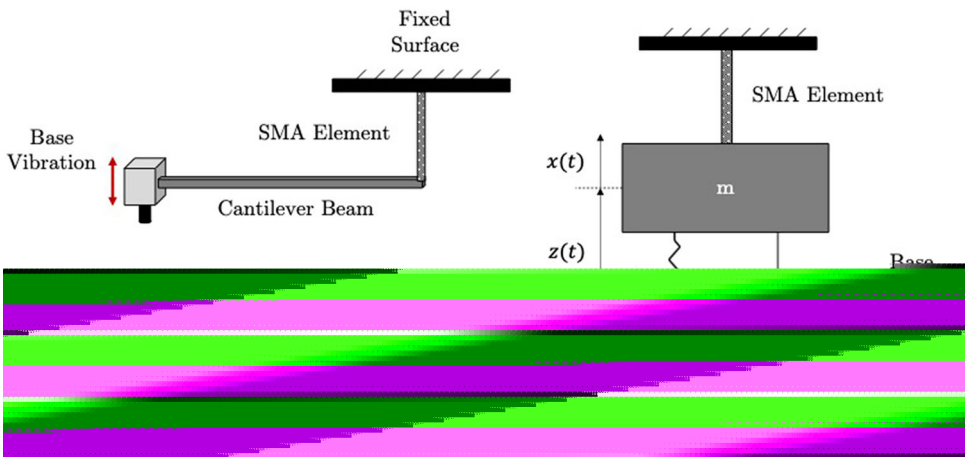

Fig. 10 SMA dynamical system represented by an oscillator: **a** cantilever beam connected to an SMA element and **b** single-degree of freedom SMA oscillator